An Investigation of Coils Used in Dynamic Wireless Charging for Electric Vehicles

Chen K. W. K[1] Cheng K. W. E[2]

Abstract–The dynamic charging for electric vehicles (EVs), compared with stationary charging, has become an essential research direction for release users from long parking time. In this paper, the coupling theories of coils are analyzed in aspects of shapes, misalignment. The considerations of coils and ferrites when designing the dynamic wireless charging system for EVs are indicated by simulation results. A wireless charging platform based on inductive coupled power transmission is presented, and the analyses are proved in hardware. The power efficiency of the proposed system is up to 82.29% after improvement.

Keywords–Wireless power transfer, electric vehicles, coupling theory

I. INTRODUCTION

The wireless power transfer, also known as wireless charging in practice, has been a hot topic and gained much attention from governments, research groups and companies all over the world. The main process of this technology is to transfer energy from power source to electric load over an air gap. It is also developed in electric vehicle charging recently and wildly.

In the last 20 years this technology once again sparked the interest of researches around the world. At the University of Hong Kong, Dr. Ron Hui and his team performed research on planar low power inductive battery chargers based on a low power printed circuit board technology [1-2]. Almost at the same time, in Auckland New Zealand, Dr. Covic and Dr. Boys started looking into high power WPT applications for mostly static charging. They have published numerous patents and journal papers, in order to describe and to highlight multiple aspects of this technology, ranging anywhere from power electronics to various circuit topologies and coil designs and optimizations [3-7].

The dynamic charging, which allows the EV can get recharged without any parking time, gets its research popularity increasingly. The significant breakthrough in the development of this technology was made by many research groups and companies. One of them was the Korea Advanced Institute of Science and Technology (KAIST), who built a On-Line Electric Vehicle (OLEV) which can transfer 60 kW of power to the busses, and 20 kW to the SUV's with efficiencies of 70% and 83% respectively [8].

However, the power efficiency of wireless charging for EVs is still not satisfied if considering worldwide using. For better understanding the factors influencing the charging process, the coupling theory is introduced. The shapes of coils and ferrites and the misalignment between emitters and receivers are the key to study the coupling.

For coil design and its optimization, reference [9] proposed an asymmetric coil sets for EV, which achieved a stationary wireless charging system with 75% power efficient and large tolerance when the horizontal displacement happens. Although this paper gives an improved coil design, it not starts from the coupling theory. Reference [10] proposed a dynamic charging system, which consists of multi-output circuits and circular pads. It analyzes the model using coupling theory, but only the interval distance is set to be a variable when compares the situation.

In this paper, the coupling theory based on basic charging process is analyzed. The mathematic models are built and their simulation results are followed, considering the shapes of coils, vertical and lateral displacement, and aspect ratio. A charging system is proposed and the experiments are also proceeded to prove the analyses in hardware. The goal is to find the considerations of coil design that helps to improve lateral tolerance and save materials.

II. COUPLING THEORY OF COUPLED COILS

1. Circular Coils

1.1. Self Inductance

The placement of coupled circular coils is depicted in Fig. 1, where R_1 and R_2 is the radius of primary and secondary coils respectively, and the *t* is the lateral misalignment while h is the interval in vertical direction.

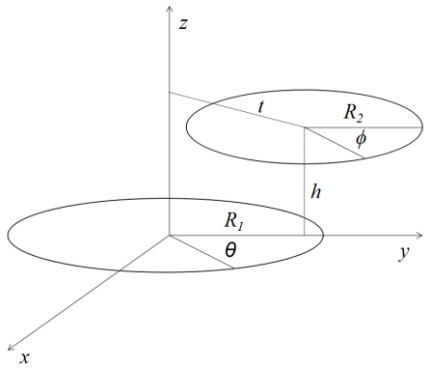

Fig. 1: Relative position of circular coils

As mentioned in the case study of inductance calculation [11], the self inductance is given by double integral Neuman formula as:

$$L_e = \frac{\mu}{4\pi}\oint_1\oint_2 \frac{d_{l_1} d_{l_2}}{r} = \frac{\mu}{4\pi}\int_0^{2\pi} d_\theta \int_0^{2\pi} \frac{R(R-r)\cos\varphi}{\sqrt{R^2+(R-r)^2-2R(R-r)\cos\varphi}} d_\varphi \quad (1)$$

Power Electronics Research Center, Department of Electrical Engineering, The Hong Kong Polytechnic University, Hong Kong
E-mail: [1]16091043g@connect.polyu.hk [2]eeecheng@polyu.edu.hk

where μ is the relative permeability of the medium.
In common cases, the radius of circle filament is much less than the curvature radius of coil, and the current is mainly distributed in the wire cross section [12]. Therefore, the internal self inductance when there is only one turn is given by:

$$L_i = \frac{\mu}{8\pi}(2\pi R) \tag{2}$$

1.2. Mutual Inductance
Based on the model shown above, we assume that R_1 and R_2 are the vectors of the primary and secondary circles. They are given by:

$$R_1 = R_1\cos\theta \boldsymbol{x} + R_1\sin\theta \boldsymbol{y} \tag{3}$$

$$R_2 = R_2\cos(\theta+\varphi)x + \left[R_2\sin(\theta+\varphi)+t\right]y + hz \tag{4}$$

$$|R_2\text{-}R_1| = \sqrt{\left[R_2\cos(\theta+\varphi)\text{-}R_1\cos\theta\right]^2 + \left[R_2\sin(\theta+\varphi)+t-R_1\sin\theta\right]^2 + h^2} \tag{5}$$

$$d_{l_1}\cdot d_{l_2} = R_1R_2\cos\theta d_\theta d_\phi \tag{6}$$

The case without lateral misalignment is simply given in [13] based on Neumann formula:

$$M = \frac{\mu}{4\pi}\int_0^{2\pi} d_\theta \int_0^{2\pi} \frac{R_1R_2\cos\varphi}{|R_2-R_1|} d_\varphi \tag{7}$$

Lateral and angular misalignment brings more complicated parameters considered in the computation process. An improved calculation method, which is named Magnetic Vector Potential Approach, is proposed in [14]. The situation of misalignment is considered. Based on [15], the equation for calculating the mutual inductance between filamentary coils with misalignment is given by：

$$M = \frac{2\mu}{\pi}\sqrt{R_1R_2}\int_0^{\pi} \frac{\left(\cos\theta - \frac{t}{R_2}\cos\phi\right)}{k\sqrt{V^3}} d_\phi \tag{8}$$

2. Rectangular Coils
2.1 Self Inductance

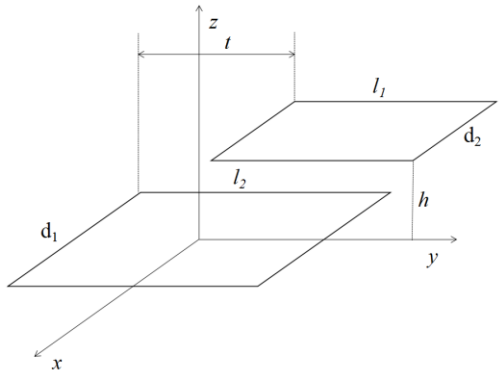

Fig. 2: Relative position of rectangular coils

To accurately compute the self-inductance of a rectangular coil, the magnetic field produced by a current element should be considered. Assuming that the current element has an unit length, the flux density generated by a straight line is given by Biot-Savart Law as:

$$B = \frac{\mu I}{4\pi\rho}\left[\frac{d-x}{\sqrt{\rho^2+(d-x)^2}} + \frac{d+x}{\sqrt{\rho^2+(d+x)^2}}\right] \tag{9}$$

The relative position of two coupled The relative position of two coupled rectangular coils has been illustrated in Fig. 2 , where l_1 and l_2 are the lengths of two coils, and d1 and d2 are their widths. And h is the vertical interval and t is the horizontal displacement, and r is the radius cross section of the winding wire. In this model, the turn of filament winding is assumed to be one for simple expression.
According to flux linkage method [16], the external self-inductance of rectangular coil can be expressed as:

$$\begin{aligned} L_e = {} & \frac{\mu}{\pi}\left[2\sqrt{(d_1-r)^2+(l_1-r)^2} - \sqrt{(d_1-r)^2+r^2} - \sqrt{(l_1-r)^2+r^2} + \sqrt{2}r + r\ln\left(\sqrt{2}-1\right)\right] \\ & + (d_1-r)\left[\ln\left(\frac{\sqrt{(d_1-r)^2+(l_1-r)^2}-(d_1-r)}{l_1-r}\right) - \ln\left(\frac{\sqrt{r^2+(d_1-r)^2}-(d_1-r)}{r}\right)\right] \\ & + (l_1-r)\left[\ln\left(\frac{\sqrt{(l_1-r)^2+(d_1-r)^2}-(l_1-r)}{d_1-r}\right) - \ln\left(\frac{\sqrt{r^2+(l_1-r)^2}-(l_1-r)}{r}\right)\right] \\ & - r\left[\ln\left(\frac{\sqrt{r^2+(l_1-r)^2}-r}{l_1-r}\right) - \ln\left(\frac{\sqrt{r^2+(d_1-r)^2}-r}{d}\right)\right] \end{aligned} \tag{10}$$

Because the radius of wire is much smaller than the one of coil radius, so we have internal self-inductance as:

$$L_i = \frac{\mu}{8\pi}(2l_1+2d_1) \tag{11}$$

2.2 Mutual Inductance
The mutual inductance of coils with rectangular shape is simpler to be computed than coupled circular coils. The result could be the summation of the mutual inductance of four different edges. As illustrating in the rectangular coordinates, we could have the equation of elements in primary coil and secondary coil, which is given by:

$$d_{l_1} = a_1\boldsymbol{x} + b_1\boldsymbol{y} - c_1\boldsymbol{x} - d_1\boldsymbol{y} \tag{12}$$

$$d_{l_2} = a_2\boldsymbol{x} + b_2\boldsymbol{y} - c_2\boldsymbol{x} - d_2\boldsymbol{y} \tag{13}$$

According to Neumann formula, the mutual inductance between one of edges (a_1 and a_2) is given by:

$$M_{a_1a_2} = \frac{\mu}{4\pi}\iint_{l_2l_1}\frac{d_{l_1}d_{l_2}}{|\boldsymbol{r_2}-\boldsymbol{r_1}|} = \frac{\mu}{4\pi}\int_{-d}^{d}\int_{-e}^{e}\frac{d_{x_1}d_{x_2}}{\sqrt{(x_2-x_1)^2+h^2+(l_1-l_2+t)^2}} \tag{14}$$

Using the same equation, we could simply add the mutual inductance of other edges and get the total mutual inductance (the mutual inductance of two orthogonal edges is equal to zero):

$$M = M_{a_1a_2} + M_{b_1b_2} + M_{c_1c_2} + M_{d_1d_2} + M_{a_1c_2} + M_{a_2c_1} + M_{b_1d_2} + M_{b_2d_1} \tag{15}$$

III. Coupling Coefficient In Different Situations

1. Coupling Coefficient v.s. Vertical Misalignment When Different Coils are Used

In this part, the radius of circular coils, both primary and secondary coils, is set to be 20mm. Meanwhile, the width and length of every rectangular coil is 40mm in order to be the similar scale with circular ones. The lateral and horizontal displacements are ignored, and the vertical distance between primary and secondary coils is varied from 10mm to 40mm.

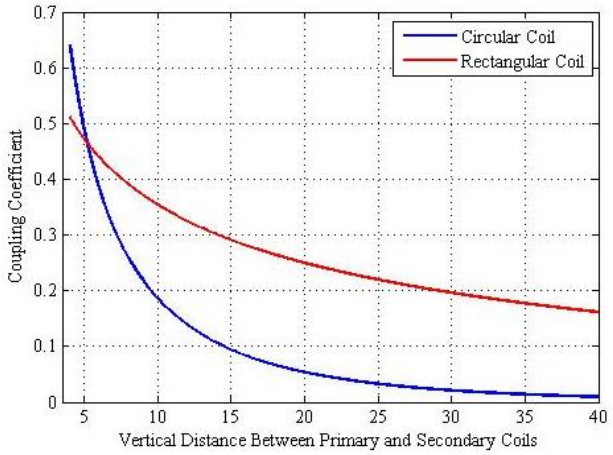

Fig. 3: Coupling coefficient v.s. vertical distance

The Fig. 3 shows the relationship between vertical distance h and coupling coefficient K. The blue and red lines are the result of circular coils and rectangular coils, respectively.
The circular coil has higher coupling coefficient when the vertical distance is lower than 5.3mm, approximately, but it will decrease rapidly after the distance become large. However, the rectangular coil will have much more slow reduction.

From the analysis, the reason why the circular coils are more widely adopted in litter air gap situation, such as cell phone charging, is obvious. But in the case of EV charging, the rectangular coils are more fit for air gap situation.

2. Coupling Coefficient v.s. Aspect Ratio
The aspect ratio can be expressed as followed:

$$m = l / d \tag{16}$$

To be comparable, the width is constant at 40mm in calculation, while length varies from 1mm to 80mm. The air gap, which is known as h, is 15mm.

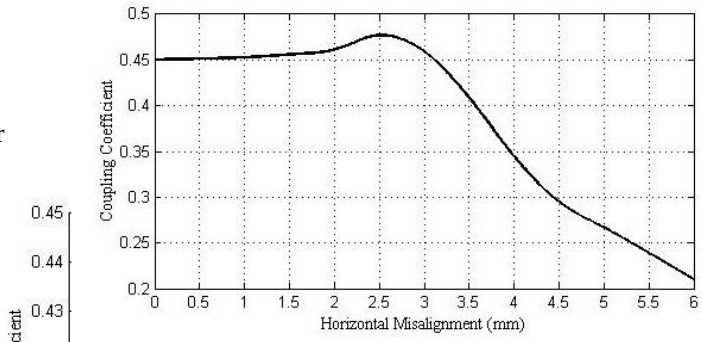

Fig. 5: Coupling coefficient v.s. horizontal displacement

According to (14) and (15), the curve of coupling coefficient can be drafted and shown in Fig. 4. The coupling coefficient is small when the aspect ratio is small. When m is smaller than 0.25, the coupling coefficient increases rapidly with the rocket of length. But after the aspect ratio come to 0.5, the increasing trend of coupling coefficient becomes slow. When the length is 20mm and 40mm, the coupling coefficient is approx. 0.4342 and 0.4358, respectively.

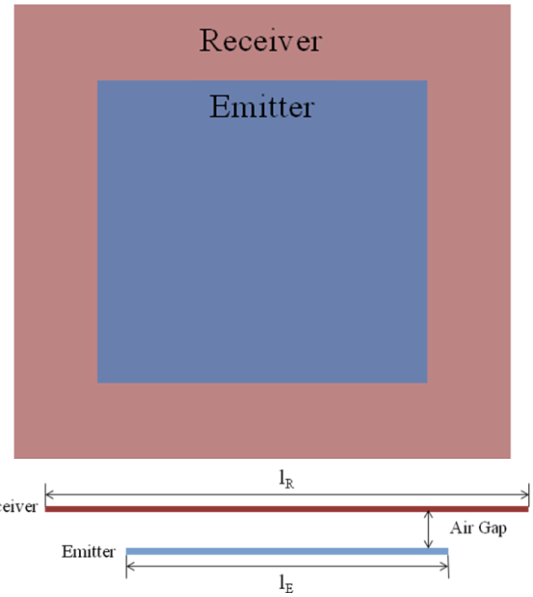

Fig. 6: Improved design of rectangular coils

Hence, for saving materials while maintaining the efficiency, the aspect ratio can be set as 0.5 when designing the coils.

3. Coupling Coefficient v.s. Horizontal Misalignment Based on Rectangular Coils

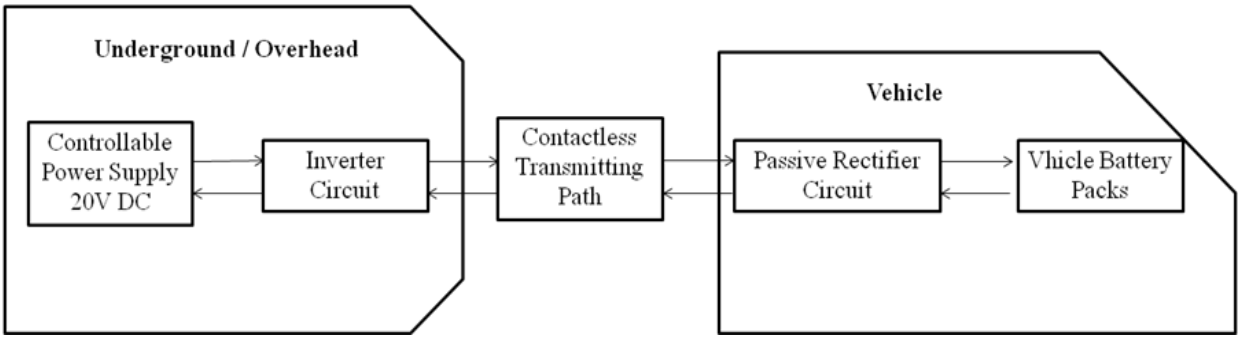

Fig. 7: Diagram of main charging circuit

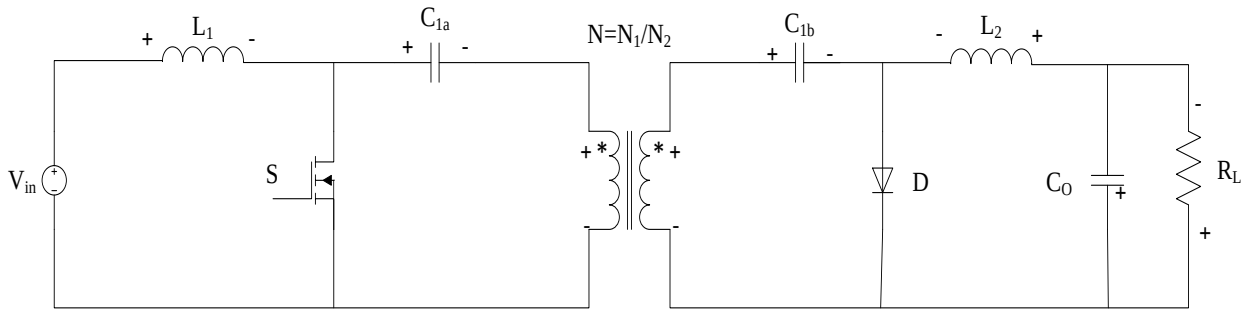

Fig. 8: Topology of main circuit

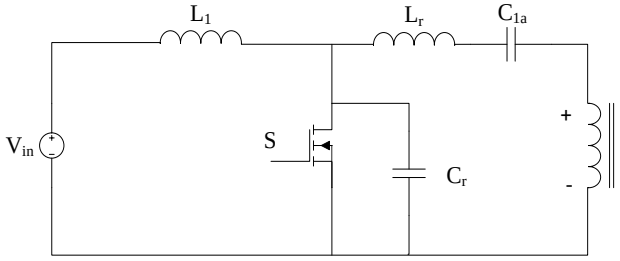

Fig. 9: Inverter with ZVS circuit

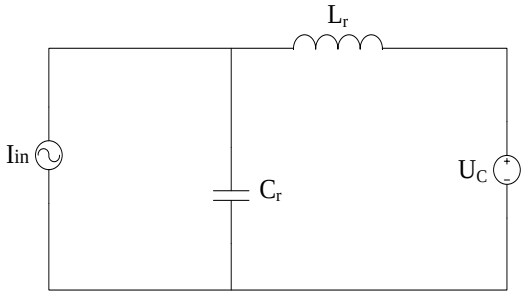

Fig. 10: ZVS Cuk Converter Equivalent Circuit

Similar to last part, the coupling coefficient is calculated when the horizontal misalignment happens when two coupled rectangular coils are used. The main parameters of coil size are also following the last section. The vertical distance h is 5mm. The horizontal displacement will vary from 0mm to 6mm in this research, while the length is set as 10mm. The result is depicted in Fig. 5.

There is a peak of coupling when the horizontal misalignment happens. After this peak, the coefficient will decrease rapidly. It indicates that when designing the system, the receiver coil should cover the emitter but in a suitable ratio, as the power transferred to second side is maximumed while the material is saved. The design consideration is illustrated in Fig. 6.

The l_m is the reluctant length of receiver, and l_m is equal to the half of the length of the emitter coil.

IV. WORKBENCH BUILDING

Fig. 7 shows the diagram of main charging circuit, the wireless charging path is the air gap which simulates the distance from vehicle chassis to the embedded emitter underground.

The topology of main circuit, including the inverter and rectifier, is shown in Fig. 8. To avoid the peak times of voltage over the switch and reduce swtiching loss, a simple Zero-Voltage-Switching circuit is implemented in the inverter, which can be seen in Fig. 9.

To design the resonant circuit, the equivalent circuit is drwan in Fig. 10. When the switch S is off and if L_1 has enough inductance, the power source and L_1 can be seen as a constant current source. Meanwhile, the diode in secondary side is working in freewheel operation, and the capacitor C_2 can be reflected into primary side. Thus, the From the equivalent circuit, the equations below can be extracted:

$$\begin{cases} I_{Cr} = C_r \dfrac{dU_{Cr}}{dt} \\ I_{Cr} = I_{in} + I_{Lr} \\ U_C - U_{Cr} = L_r \dfrac{di_{Lr}}{dt} \end{cases} \tag{17}$$

The initial conditions are as followed:

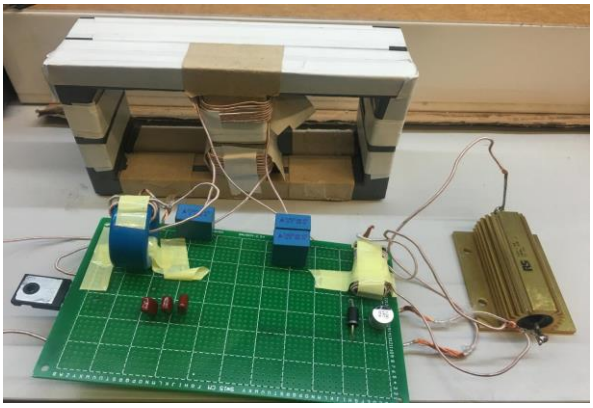

Fig. 11: Workbench of charging system

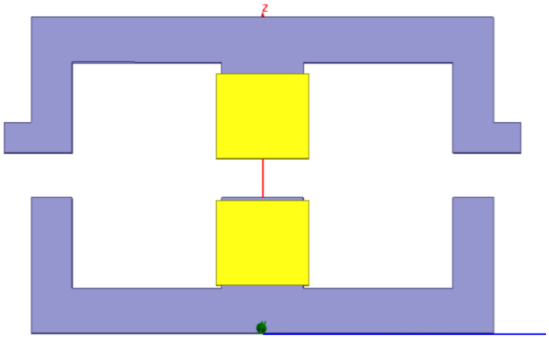

(a): No horizontal misalignment

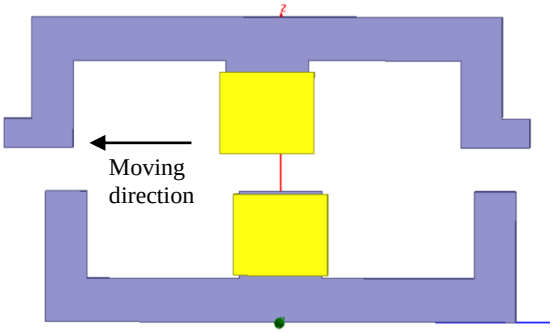

(b): Horizontal misalignment happens

Fig. 12: Experiment of horizontal misalignment

$$\begin{cases} U_{Cr}(0) = 0 \\ I_{Cr}(0) = I_{in} + I_{Lr0} \end{cases} \tag{18}$$

Where I_{Lr0} is the initial current of inductor.

I_{Lr0} can be decided by output current as:

$$I_{Lr0} = \frac{I_o}{n} \tag{19}$$

Based on the equations (17), (18) and (19), the voltage over resonant capacitor can be calculated:

$$U_{Cr} = \sqrt{U_C^2 + I_{Cr0}^2 \frac{L_r}{C_r}} \sin(\omega t - \theta) + U_C \tag{20}$$

Where the phase angle and angular speed are as followed:

Table 1: Parameters of Components

Component	Main Value
L_1	$50\mu H$
L_2	$10\mu H$
L_r	$10\mu H$
C_1	$1\mu F$
C_2	$2\mu F$
C_r	$1\mu F$
C_o	$100\mu F$
V_{in}	$20V$ DC

$$\begin{cases} \theta = \text{arctg} \dfrac{U_C}{I_{Cr0}\sqrt{L_r/C_r}} \\ \omega = \sqrt{\dfrac{1}{L_r C_r}} \end{cases} \tag{21}$$

Starting from $t = 0$, the first time and second time when the U_{Cr} is crossing zero are:

$$\begin{cases} t_1 = (\pi + 2\theta)/\omega \\ t_2 = 2\pi/\omega \end{cases} \tag{22}$$

Between t_1 and t_2, the switch can achieve zero-voltage switching. From the analysis, it can be concluded that this circuit have a simple structure with easy control and less loss in components. If the inductance of transformer can be used as resonant inductor L_r, the additional components are only resonant capacitor. The resonant capacitor C_r is paralleled with switch S, absorbing the over-voltage and the high frequency ripple waves over the switch at the very time of turning off. Due to the time limitation allowing ZVS, this simple ZVS topology is suitable for stable loads situation, where the duty time of gate control signal is nearly constant.

The paremeters of all components are listed in Table 1. The ratio N is 1, and the voltage conversion of the converter is 1 consequently .

V. Experimental Results

As for proving the simulation results, the experiments are proceeded in a low power workbench, with 80kHz frequency and 5mm air gap. The width and length of the center rectangular coils are both 30mm. The workbench is shown in Fig. 14. When there is no later misalignment and the load is a 9Ω resistor, the input power is 48W, and the output power is 32.11W. The power efficiency is 66.89%. As the rectangular coil is more suitable for dynamic charging, the design consideration of it is more important. For improve the tolerance of later displacement, the design of the coil and its position is the very factors ferrites are used. Their placement is depicted in Fig. 12, where the lower one is the emitter and above it is receiver. The yellow part is the coils twined on the ferrites.

The results of experiments are presented in a oscilloscope, where the Channel 1 (yellow lines) is the output voltage, and Channel 2 (blue lines) represents the switching frequency and Channel 3 (purple lines) is the voltage over the switch S. From the results of scope, it is obvious that

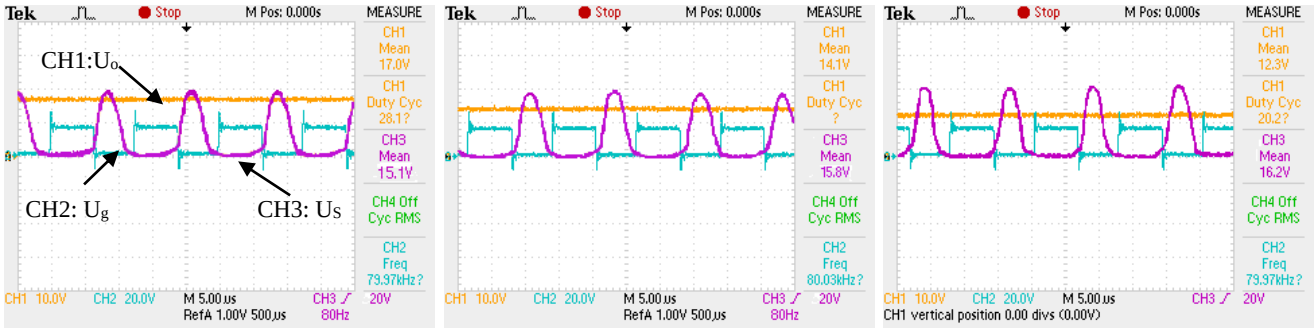

(a): Experiment result (Uo =17.0V) (b): Experiment result (Uo =14.1V) (c): Experiment result (Uo =12.3V)

Fig. 13: Output voltage of charging system (CH1: 2.5V/Unit, CH2: 4V/Unit, CH3: 4V/Unit)

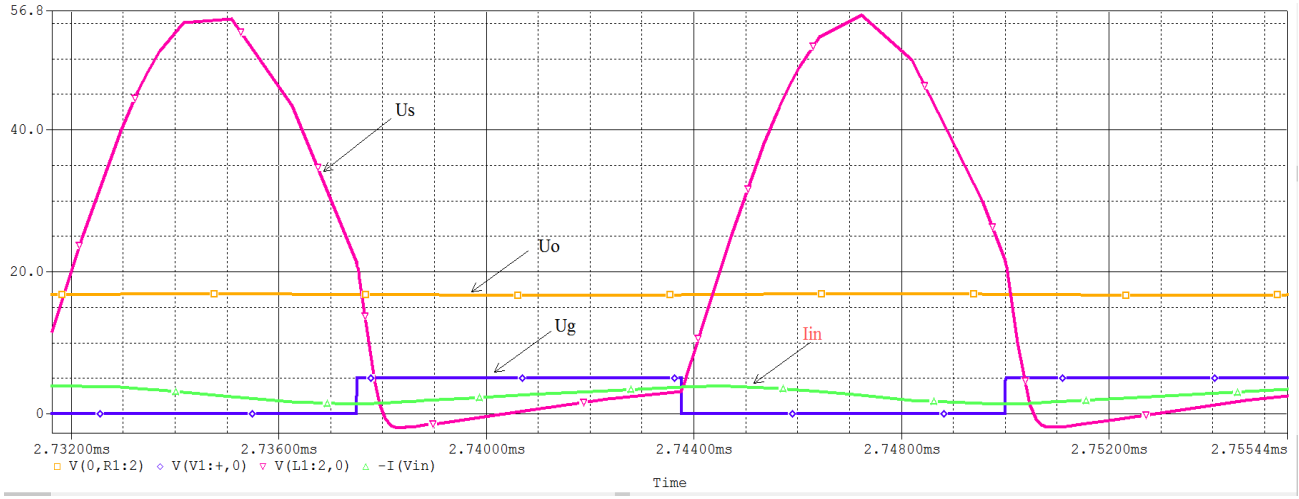

(a) R=9Ω

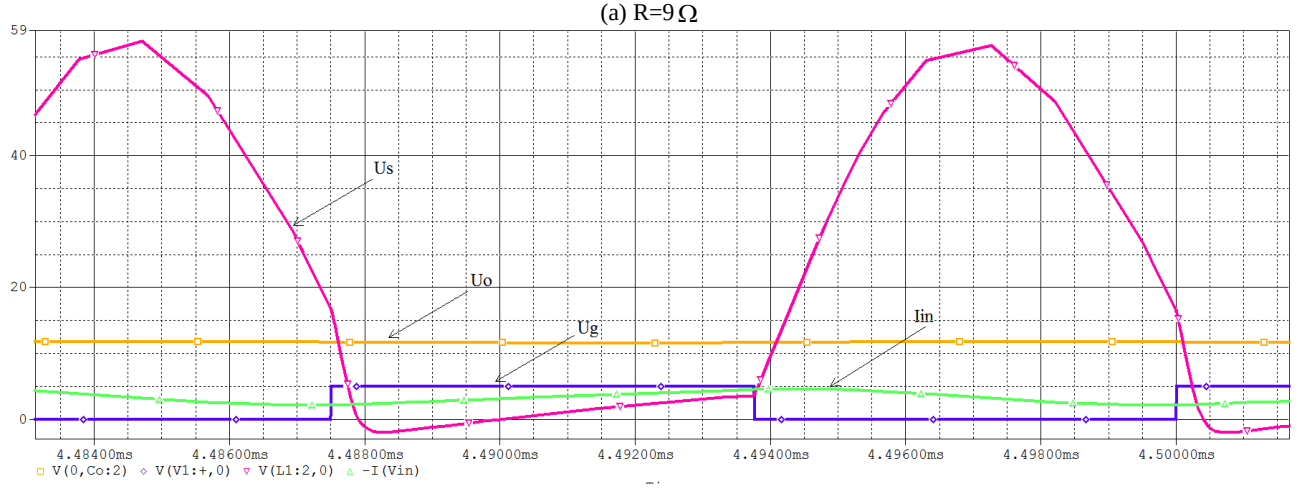

(b) R=2.5Ω

Fig. 15: System simulation results

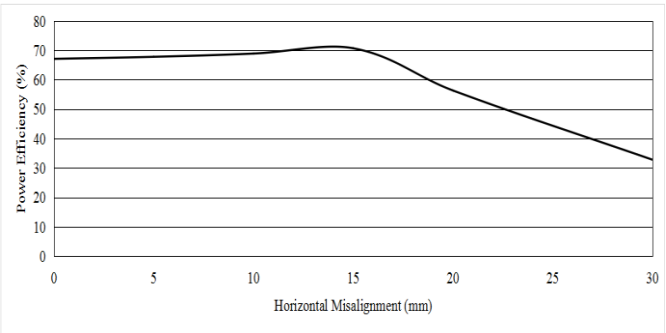

Fig. 14: Experiment results of power efficiency v.s. horizontal misalignment

the voltage over the switch will be reduced to zero just before it is turned on again. It proves that the ZVS is achieved and the resonant circuit is working effectively.

The outputs are sampled when the lateral movement distance is changing from 0mm to 30mm, and Fig. 13 shows three of the sampled results detected in the oscilloscope. The power efficiency curve which is changing with horizontal misalignment is shown in Fig. 14. From the results, it is obvious that the power efficiency has its peak when the horizontal misalignment is 15mm, which proves that the tolerance of the lateral displacement can be improved when the secondary coil covers the emitter coil.

The highest efficiency of the platform is 66.89%, which is not satisfied due to the non-matching load. Fig. 15 (a) and

(b) show the simulation results in PSPICE, when the load is 9Ω and 2.5Ω resistor respectively. When the 9Ω is as the matched loading and the coupling coefficient is 0.632, the output voltage is 17.3V which is also presented in experiment. The output voltage is 33.25W, and the power efficiency is 66.51%. After matching the load by using 2.5Ω resistor, the power efficiency is improved to 82.29% in the same coupling, where the output voltage is heightened to 57.6W.

VI. Conclusion

The coupling theory of EV dynamic wireless charging is discussed. The factors, shapes of coils, vertical and horizontal misalignment and aspect ratio are considered based on mathematic models. The simulation results are following the analyses. Based on the results, several conclusions of coil design are indicated as followed:

1. The rectangular coils are more suitable for EV dynamic charging.
2. The aspect ratio 0.5 (length/width) is helpful for saving materials while maintaining the power efficiency.
3. The receiver coils should cover the emitters with proper ratio (l_m = Emitter coils length/2).

The experiments are proceeded in a 80kHz low power workbench successfully. The ZVS resonant circuit is achieved successfully as to reduce the switch loss. The considerations introduced former are proved. The efficiency of the designed platform can be up to 82.29% after using well-matched load.

Reference

[1] Tang, Sc, Ron Hui, Sy, and Chung, Hsh. "A Low-profile Power Converter Using Printed-circuit Board (PCB) Power Transformer with Ferrite Polymer Composite." 16, no. 4 (2001): 493-498.

[2] "Univ City Hong Kong Files European Patent Application for Planar Inductive Battery Charger." Global IP News. Electrical Patent News (New Delhi), January 16, 2014.

[3] Hao Hao, Covic, & Boys. (2014). "A Parallel Topology for Inductive Power Transfer Power Supplies." Power Electronics, IEEE Transactions on, 29(3), 1140-1151.

[4] Budhia, M., Boys, J.T., Covic, G.A., and Chang-Yu Huang. "Development of a Single-sided Flux Magnetic Coupler for Electric Vehicle IPT Charging Systems.(inductively Power Transfer)(Technical Report)." IEEE Transactions on Industrial Electronics 60, no. 1 (2013): 318.

[5] Keeling, N.A., G.A. Covic, and J.T. Boys. "A Unity-Power-Factor IPT Pickup for High-Power Applications." Industrial Electronics, IEEE Transactions on 57, no. 2 (2010): 744-751.

[6] Kissin, Michael L G, Grant A Covic, and John T Boys. "Steady-State Flat-Pickup Loading Effects in Polyphase Inductive Power Transfer Systems." Industrial Electronics, IEEE Transactions on 58, no. 6 (2011): 2274-2282.

[7] Huang, C.-Y., Boys, J. T., and Covic, G. A. "LCL Pickup Circulating Current Controller for Inductive Power Transfer Systems." IEEE Transactions on Power Electronics 28, no. 4 (2013): 2081-2093.

[8] Kong, Sunkyu, Bae, Bumhee, Jung, Daniel H., Kim, Jonghoon J., Kim, Sukjin, Song, Chiuk, Kim, Jonghoon, and Kim, Joungho. "An Investigation of Electromagnetic Radiated Emission and Interference From Multi-Coil Wireless Power Transfer Systems Using Resonant Magnetic Field Coupling." IEEE Transactions on Microwave Theory and Techniques 63, no. 3 (2015): 833-846.

[9] Choi Su Y., Jin Huh, Woo Y. Lee, and Chun T. Rim. "Asymmetric Coil Sets for Wireless Stationary EV Chargers with Large Lateral Tolerance by Dominant Field Analysis." Power Electronics, IEEE Transactions on 29.12(2014): 6406-6420.

[10] Zhang X., Yuan Z. Y., Yang Q. X., Li Y. J., Zhu J. G., and Li Y. "Coil Design and Efficiency Analysis for Dynamic Wireless Charging System for Electric Vehicles." Magnetics, IEEE Transactions on 52.7 (2016):1-4.

[11] Shatz Lisa F., and Christensen Craig W. "Numerical Inductance Calculations Based on First Principles." PLoS ONE 9, no. 11 (2014): PLoS ONE, Nov 17, 2014, Vol.9(11).

[12] Yao Luo and Baichao Chen. "Improvement of Self-Inductance Calculations for Circular Coils of Rectangular Cross Section." Magnetics, IEEE Transactions on 49, no. 3 (2013): 1249-1255.

[13] Babic S., C. Akyel and S.J. Salon. "New Procedures for Calculating the Mutual Inductance of the System: Filamentary Circular Coil-massive Circular Solenoid." Magnetics, IEEE Transactions on 39, no. 3 (2003): 1131-1134.

[14] Amos Anele O., Hamam Ykandar, Alayli Yasser, and Djouani Karim. "Computation of the Mutual Inductance between Circular Filaments with Coil Misalignment." AFRICON, 2013, 2013, 1-5.

[15] Anele, Hamam, Chassagne, Linares, Alayli, and Djouani. "Computation of the Mutual Inductance between Air-Cored Coils of Wireless Power Transformer." Journal of Physics: Conference Series 633, no. 1 (2015): 6.

[16] Snyder J. N. "Inductance Calculations Working Formulas and Tables (Book Review)." Mathematics of Computation 18, no. 85 (1964): 164.